frontiers | Frontiers in Materials

TYPE Original Research
PUBLISHED 26 June 2023
DOI 10.3389/fmats.2023.1038574

OPEN ACCESS

EDITED BY
Gürel Cam,
Iskenderun Technical University, Türkiye

REVIEWED BY
Citlalli Gaona-Tiburcio,
Autonomous University of Nuevo León, Mexico
Luca Pezzato,
University of Padua, Italy

*CORRESPONDENCE
Myeonghoon Lee,
leemh@kmou.ac.kr

RECEIVED 20 October 2022
ACCEPTED 14 June 2023
PUBLISHED 26 June 2023

CITATION
Seo B, Kim Y, Oh S, Lee S and Lee M (2023), Corrosion behaviors of super austenitic stainless steel weldment by GTAW welding for ships desulfurization system.
Front. Mater. 10:1038574.
doi: 10.3389/fmats.2023.1038574

Corrosion behaviors of super austenitic stainless steel weldment by GTAW welding for ships desulfurization system

Beomdeok Seo[1], Yongseong Kim[1], Seok Oh[1], Seunghyo Lee[2] and Myeonghoon Lee[1]*

[1]Division of Marine Engineering, Interdisciplinary Major of Maritime AI Convergence, Korea Maritime and Ocean University, Busan, Republic of Korea, [2]Department of Ocean Advanced of Materials Convergence Engineering, Korea Maritime and Ocean University, Busan, Republic of Korea

This study aims to clarify how filler-typed metals which were ERNiCrMo-3 and ERNiCrMo-4 affect corrosion resistance characteristics in the weldment of super austenitic stainless steel joints under the simulated desulfurization environment for ships. The desulfurization environment includes high temperature, chlorides, and acidic conditions, which, inevitably, can cause severe corrosion to great extent. For exact clarification, the variations of microstructure and the composition distribution in the weldment before and after welding was examined by using scanning electron microscope and energy dispersive X-ray spectroscopy. Then, the corrosion resistance characteristics were comparatively evaluated through the cyclic potentiodynamic polarization test together with potential measurement under the desulfurization simulated environments. In addition, the correlation between passive film and corrosion resistance characteristics was investigated after identifying the formed features of the passive film through the X-ray photoelectron spectroscopy analysis. Through these studies, it made certain, ERNiCrMo-4 filler metal with high Mo content is advantageous for the formation of MoO_3 oxide on the surface, which belongs to form a stable passive film and maintains the corrosion resistance characteristics under the simulated desulfurization environment.

KEYWORDS

ships desulfurization system, super austenitic stainless steel, weldment corrosion, ERNiCrMo-3, ERNiCrMo-4

1 Introduction

The socio-economic costs increased only from air pollution attributable to particle matters from the cruising vessels tended to have continuously grown as self-explanatory. In maritime sector alone, International Maritime Organization under the United Nations confronted imminent counteraction to control the air quality issue and commenced to enforce reduction of sulfur content emission from marine fuel oil to 0.5% or less since 1 January 2020 (Aulinger et al., 2016; Makkonen and Repka, 2016). One of the responses to these strong environmental regulations is to install desulfurization equipment inside a ship, such as scrubbers, to reduce the level of sulfur oxide in the gas emitted after the use of heavy fuel oil (Kallinikos et al., 2010; Ye et al., 2013).

However, when to remove contaminants through the desulfurization process, not only an acidic solution containing sulfides as well as chlorides is formed but also materials used in

the equipment are exposed to an extremely corrosive environment due to an operating environment where dry and wet methods are alternated during high temperature (Kallinikos et al., 2010). The serious corrosion problem caused from this has been reported as the most significant problem in maintaining the reliability and stability of the equipment (Zhu et al., 2015; Gong and Yang, 2018). To have this problem controlled, it is critically important to select material for desulfurization equipment with a high corrosion-resistant in a harsh corrosive environment (Aragon et al., 2009; Zhu et al., 2015; Pan et al., 2017; Gong and Yang, 2018). Several studies have been conducted to select materials suitable for desulfurization equipment, and there are guidelines for selecting materials considering the operating environment by classifying them according to temperature and chloride concentration (Paul et al., 2015; DeForce, 2017).

Among many materials, super austenitic stainless steels are a representatively material for the desulfurization equipment whose Pitting Resistance Equivalent Number (PREN) is greater than 48 (Nagarajan and Rajendran, 2009; Seifert et al., 2016). It is known to have high corrosion resistance against pitting and crevice corrosion by forming a stable passive film even in harsh environments (Stein et al., 1999; Nagarajan and Rajendran, 2009). In particular, according to the results of the corrosion resistance characteristics in the green death solution (2.2M H_2SO_4 + 0.4M HCl + 0.06M $FeCl_3$ + 0.07M $CuCl_2$), which simulated a harsh corrosive environment inside the desulfurization equipment, super austenitic stainless steel reliably maintained the corrosion resistance characteristics and was reported to be the economically best material compared to other experimental materials such as Inconel alloy 625 and Hastelloy C22 (Crum et al., 1996; Hertzman et al., 1996; Phull et al., 2000; Woo and Kikuchi, 2002; Shin, 2015).

Stainless steel parts are usually welded in many applications and conventional arc welding processes such gas metal arc welding (GMAW) and gas tungsten arc welding (GTAW) processes are widely employed in the joining of these materials (Serindağ and Çam, 2021; Serindağ and Çam, 2022a; Serindağ and Çam, 2022b; Ezer and Çam, 2022; Serindağ et al., 2022; Şenol and Çam, 2023). However, despite the excellent corrosion resistance of stainless steels, the problem of localized corrosion of the welded parts after the welding process has been continuously reported (Heino, 2000; Kang et al., 2012; Wu et al., 2019; Chacón-Fernández et al., 2022; Miranda-Pérez et al., 2023). Miranda-Pérez et al. examined the corrosion resistance of the welds of duplex stainless steels fabricated by gas metal arc welding (Miranda-Pérez et al., 2023). They concluded that higher heat input yielded the most favorable corrosion properties when exposing both a synthetic seawater solution and exposure to H_2S gas. However, prior research has failed to thoroughly explore the corrosion resistance properties of weldments in the context of desulfurization equipment environments using actual materials. Furthermore, there has been a notable lack of studies examining the relationship between weld process variables and the passive film, despite the strong correlation between corrosion resistance characteristics in weldments and the formation of a passive film.

This work describes the correlation between the filler metal type and corrosion resistance of the super austenite stainless steel weldment in a simulated environment where desulfurization equipment is employed. The electrochemical corrosion test was used for a comparative evaluation of the corrosion resistance. The influence of the components of the welding material on the passivation film formation and corrosion resistance was investigated by passive film analysis, and PREN, which was used as the standard of pitting resistance of stainless steel. Through these undertakings, we intend to present design guidelines for the selection of welding materials that can increase reliability and stability by suppressing the corrosion of welding parts of actual desulfurization equipment.

2 Experimental procedure

2.1 Materials and welding process

The base metal used in this study was 4 mm thick UNS N08367, which is a typical super austenitic stainless steel. Welding materials whose PREN is higher than that of the base metal are used considering the corrosion resistance characteristics generated due to element segregation which occurs when welding the super austenitic stainless steel. Thus, in this study, ERNiCrMo-3, which has been most widely used when welding the super austenitic stainless steel, was selected as a filler metal whilst using ERNiCrMo-4 as a comparative filler metal (Rabensteiner, 1989; Dupont et al., 2003). The specific element composition of each material is presented in Table 1. The PREN was calculated using the average composition of samples based on the following equation (Ha and Kwon, 2007).

$$PREN = \%Cr + 3.3\%Mo + 30\%N \quad (1)$$

To fabricate a specimen, butt welding was conducted as shown in Figure 1 by supplying and melting filler metals differently while performing gas tungsten arc welding (GTAW). The detailed welding parameters are shown in Table 2. Heat input was calculated by

$$Heat\ input\ (kJ/mm) = \frac{60VA}{1000v} \quad (2)$$

Where V is the voltage applied, A is the current, and v is the travel speed. The base metal belonging to super austenite stainless steel manifests a susceptibility to heat cracking; for that reason, the specific heat input was limited to 1 kJ/mm, and the inter-pass temperature was maintained at 100°C or lower (Lauro and Mandina, 2003; Sathiya et al., 2012). The shielding gas used in welding showed very high purity Argon gas of 99.999%.

2.2 Microstructural characterization

The fabricated specimen was mirror-polished using 1 μm particle diamond paste to observe the microstructure. Etching was conducted using 10 wt% oxalic acid (100 g of oxalic acid + 900 mL of distilled water) solution in accordance with ASTM A262-Practice A (Standard, 2002). The microstructure and composition were investigated using scanning electron microscopy (SEM, MIRA 3, Tescan, Czech) system coupled to an energy-dispersive spectrometer (EDS).

TABLE 1 Chemical Composition and pitting resistance equivalent number for specimens.

Base or filler metal	Chemical composition in %									
	C	Si	Mn	Cr	Mo	Ni	N	Fe	Others	PREN
UNS N08367	0.01	0.3	0.7	20.6	6.4	24.5	0.2	Bal	Cu: 0.53	48.7
ERNiCrMo-3	0.14	0.08	0.03	22.2	8.7	63.8		-	Nb: 3.36	50.8
ERNiCrMo-4	0.01	0.04	0.5	15.8	16.0	57.6		5.9	W: 3.67	68.6

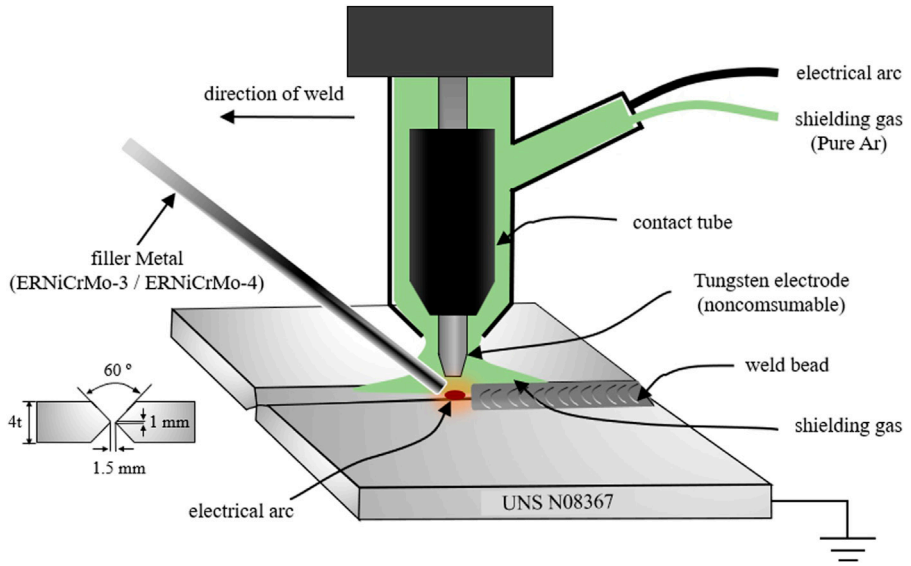

FIGURE 1
Schematic of a gas tungsten arc welding system.

TABLE 2 Welding parameters for GTAW process.

Weld pass	Current (A)	Voltage (V)	Travel speed (mm/min)	Heat input (kJ/cm)
Root	105	8.5	825	0.64
Middle & Cap	110	8.5	1460	0.38

2.3 Electrochemical corrosion tests

The corrosion resistance of the weldments (fusion zone + weld interface + base metal) was evaluated using an electrochemical corrosion test. All tests were conducted with three-electrode electrochemical tests using an electrochemical workstation (Interface 1010, Gamry, United Statesa) in a green death solution (2.2M H_2SO_4 + 0.4M HCl + 0.06M $FeCl_3$ + 0.07M $CuCl_2$), which was made without degassing it at 60°C where dew point corrosion was most likely to occur in the desulfurization equipment (Rommerskirchen et al., 2001; Kallinikos et al., 2010). A three-electrode cells was used with weldment specimens as the working electrode with 1.0 cm^2 of surface exposed to the electrolyte, a high density carbon rod as the counter electrode, and the a saturated calomel electrode (SCE) as the reference electrodes, as shown in Figure 2. The specimen was bonded together with copper wire by brazing and then mounting it on epoxy resin. The surface of the specimen was fabricated by grinding up to 2,000 grit using emery paper, and then, all the samples were ultrasonically cleaned with alcohol. To check the reproducibility, on the other hand, three measurements were conducted at the least.

The cyclic potentiodynamic polarization test was conducted according to ASTM G 61-86 (ASTM, 2001). To measure pitting potential, repassivation potential, critical current density, and to locate passive state area, the test was conducted under the desulfurization equipment environmental conditions. The cyclic potentiodynamic polarization measurements were measured from an initial potential of −100 mV vs. OCP at a scan rate of 1.0 mV/s

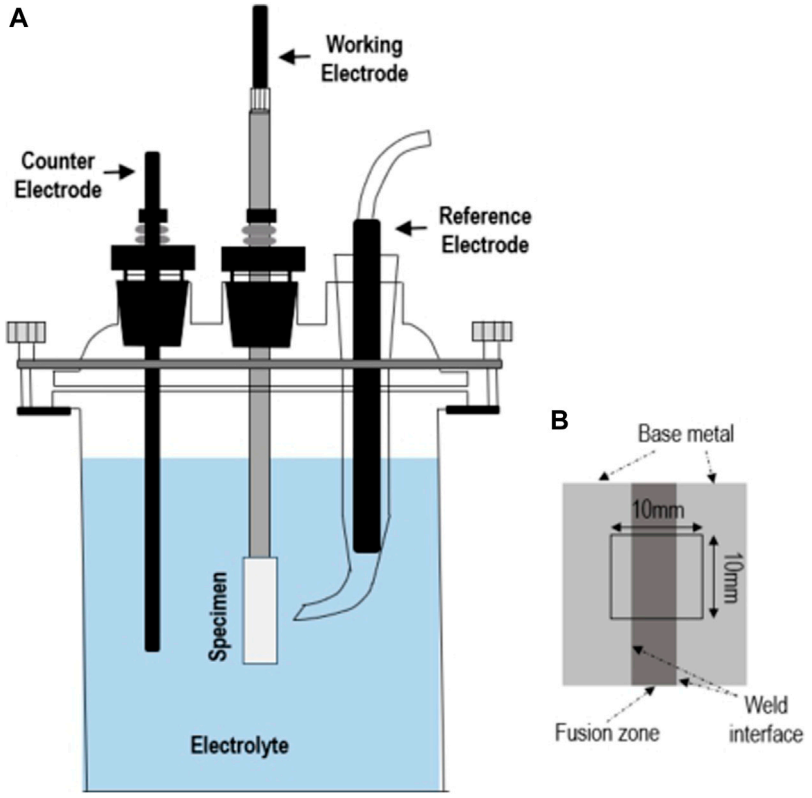

FIGURE 2
(A) Schematic diagram of the electrochemical testing cell used for corrosion testing and **(B)** schematic of the specimen used for investigating the corrosion behavior.

(Fang et al., 1995; Taheri et al., 2020; Guo et al., 2021). The scan direction was reversed at the anodic current density value of 1 mA/cm^2.

In addition, the self-activation phenomenon was observed through the open cricuit potential change from the passive into the active state via the passive-active transition region, thereby allowing for a review of the dissolution behavior and stability of the passive film in this study. To do this, a passive film was formed after applying the potential of the passive region, which was confirmed through the cyclic potentiodynamic polarization test, to the specimen in the desulfurization equipment environment for an hour. Then, the open circuit potential change was measured until the passive film was destroyed and activated while opening the circuit. Since this was conducted in an open-circuit state, it had the advantage of reducing the effect on the change of polarization or passive film caused by the general electrochemical test method.

2.4 Passive film characterization

To verify the correlation between the passive film formation and corrosion resistance characteristics, the passive film was analyzed using an X-ray photoelectron spectroscopy (XPS, ESCA 3400, Shimadzu Co., Japan). The mirror-polished specimens were immersed in the desulfurization equipment environment for 7 days and then removed from the solution. After that, the samples were gently rinsed with distilled water and dried at room temperature. The binding energy was calibrated by the C 1s peak at 284.5 eV.

3 Results and discussion

3.1 Microstructure analysis

Figures 3, 4 show the microstructure of weldments fabricated by GTAW with ERNiCrMo-3 and ERNiCrMo-4. The cross section shows the defect free weldments in the two types of fabricated specimens (Figures 3A, 4A). Figure 3B, 4B represents microstructures of the fusion zone for weldments. The microstructures show both were formed to cellular and columnar dendritic structures caused by the difference in constitutional supercooling during the coagulation process. The difference observed when constitutional supercooling was known to occur due to the change in the growth rate of the solid-liquid interface and temperature gradient (Kim et al., 2011). The width of unmixed zone of ERNiCrMo-3 is large than the ERNiCrMo-4. The formation of unmixed zone is due to different melting point and the deviation in chemical composition between the base metal and filler metal.

Figure 5 shows the analysis results of elemental composition when using an EDS according to the microstructure welded by

10.3389/fmats.2023.1038574

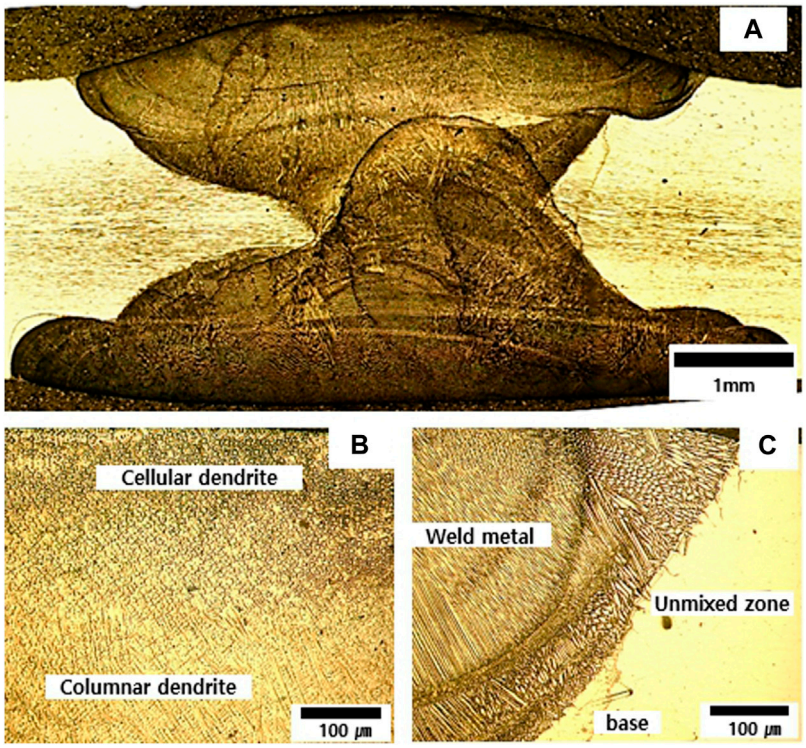

FIGURE 3
Optical images showing microstructures fabricated by ERNiCrMo-3 filler metal **(A)** cross section **(B)** fusion zone **(C)** weld interface.

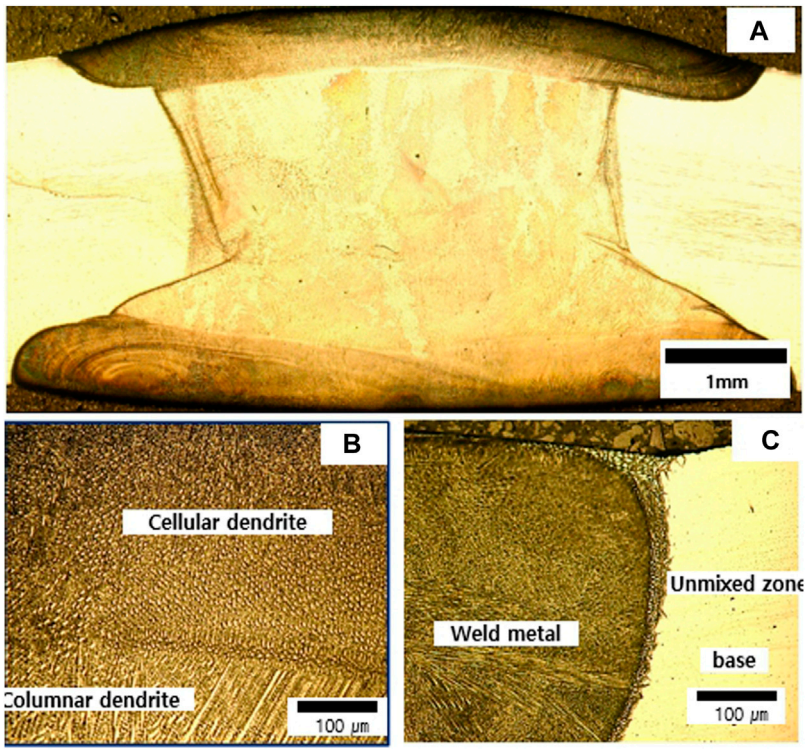

FIGURE 4
Optical images showing microstructures fabricated by ERNiCrMo-4 filler metal **(A)** cross section **(B)** fusion zone **(C)** weld interface.

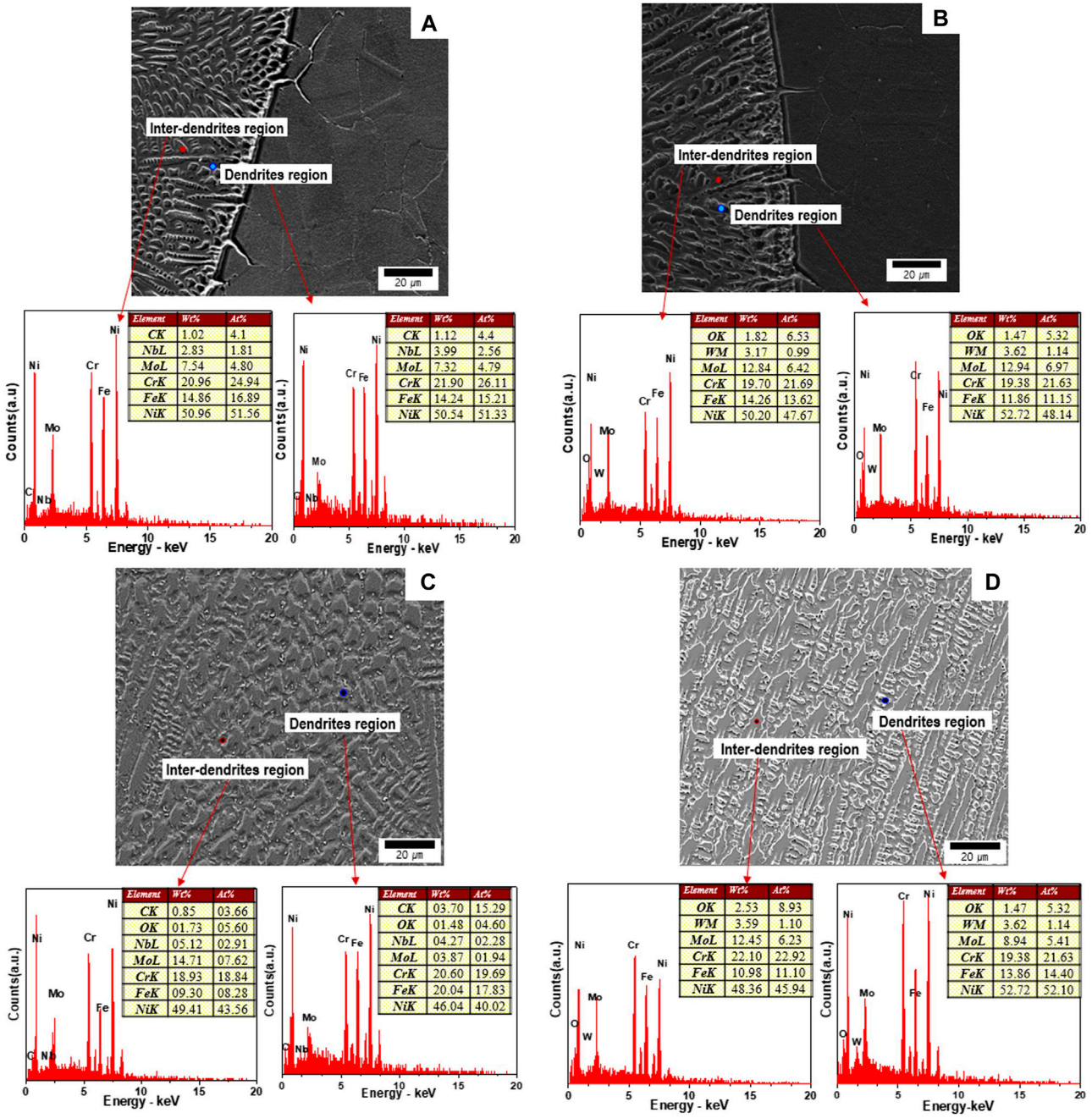

FIGURE 5
SEM and EDS point analysis on **(A)** ERNiCrMo-3 interface **(B)** ERNiCrMo-4 interface **(C)** ERNiCrMo-3 fusion zone and **(D)** ERNiCrMo-4 fusion zone.

different types of filler metals. Figure 6 shows the segregation ratio (between alloy content in inter-dendritic and dendritic solid) between elements that occurred in the solidification process after welding (Zhang and Li, 2012; Manikandan et al., 2014).

In the interface area, there is less difference in elemental compositions (Ni, Cr, and Mo) between inter-dendritic and dendritic solid for both filer metals (Figures 5A, B); the segregation ratio of most elements is distributed close to 1.0 (Figure 6A). However, in the case of the weld fusion area, it was verified that the elemental composition significantly varied according to the microstructure that occurred when implementing the solidification process after welding (Figures 5C, D). In particular, both of the two specimens demonstrated that Mo diffused toward the dendritic boundary during solidification after welding, thereby being solidified intensively while the center dendritic region manifested segregation where Mo was deficient (Figure 6B). However, the micro-segregation level showed some difference in accordance with the types of filler metals, which is illustrated clearly in Figure 6. This indicates that there was a region where the Mo content was smaller than that of the base metal in the microstructure in the weldment because the segregation occurred greatly when using ERNiCrMo-3 filler metal. On

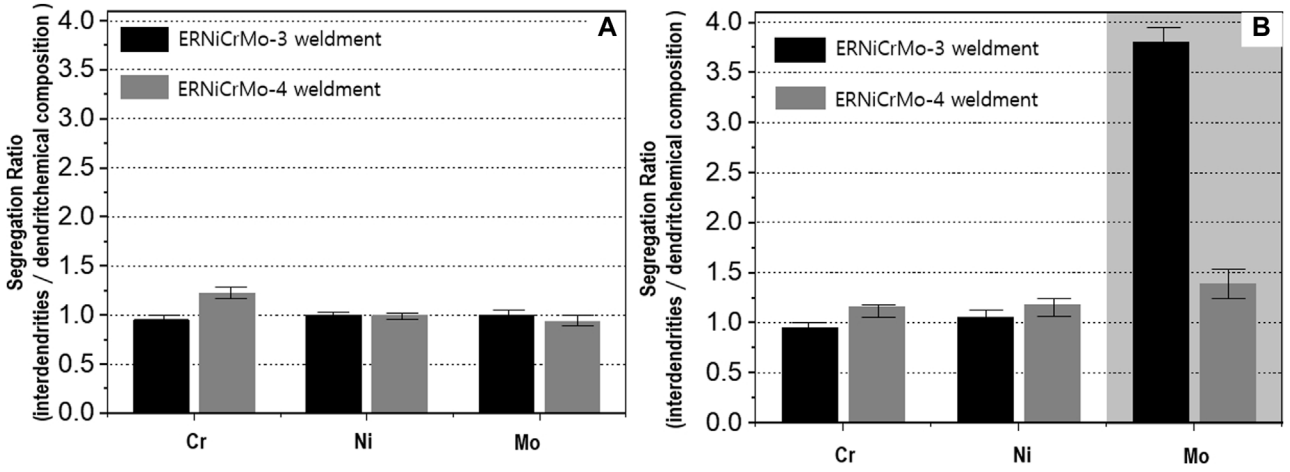

FIGURE 6
Segregation ratio of different alloying elements **(A)** weld interface **(B)** weld fusion zone.

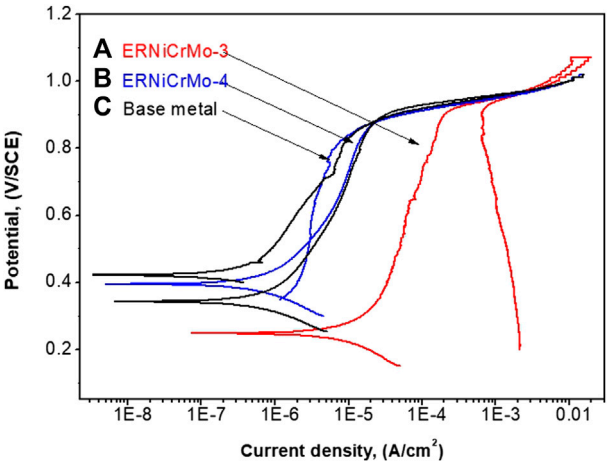

FIGURE 7
Cyclic potentiodynamic polarization curves on the specimens tested in the desulfurization equipment simulation environment at 60°C **(A)** ERNiCrMo-3 filler metal **(B)** ERNiCrMo-4 filler metal **(C)** base metal.

the other hand, when using ERNiCrMo-4, the difference observed in elemental composition was significantly small compared to using ERNiCrMo-3 filler metal. In particular, the difference in elemental composition between the microstructures will induce a difference in PREN value and thereby it appears to produce an imbalance of corrosion resistance characteristics between the microstructures.

3.2 Cyclic potentiodynamic polarization tests

Figure 7 shows the cyclic potentiodynamic polarization curves of welded joints and substrate in the desulfurization equipment simulation environment. This verified that resistance existed in the local corrosive area when comparatively evaluating the trend in the repassivation state after destroying the passive film, which was formed on the material surface. The corresponding corrosion potential (E_{corr}) and corrosion current (i_{corr}), pitting potential (E_{pit}), and repassivation potential (E_{rep}) are listed in Table 3. The E_{corr} values, after welding, all of filer metal show a lower potential than the base metal. The i_{corr} values of ERNiCrMo-3 (2.76 μA/cm^2) and ERNiCrMo-4 (0.91 μA/cm^2) were larger than those of the base metal (0.32 μA/cm^2). When the potential was in forward direction, it showed rather rapid increase in corrosion current density when the potential (E_{pit}) reached approximately similar in all specimens. This displayed the rapid destruction of the formed passive film. However, when the potential was in reverse direction, a different result was developed depending on the filler metal type. The Erep did not appear because the current density was greater in the reverse direction scanning potential curve than in the forward direction in the case of the weldment using ERNiCrMo-3 filler metal. That indicates that repassivation did not occur, and the localized corrosion progressed (Esmailzadeh et al., 2018). On the other hand, the base metal and the weldment using ERNiCrMo-4 filler metal showed an appearance of the E_{rep} as the current density was rapidly reduced when the potential was scanned in the reverse direction. This was because the damaged passive film was rapidly reactivated, caused by the suspended result of the local corrosion growth (Esmailzadeh et al., 2018). Figure 8 shows the surface condition with EDS mapping results of each specimen observed after the cycle potentiodynamic polarization test. As shown in Figure 8A, localized corrosion occurred intensively in the dendritic region. On the other hand, in the case of ERNiCrMo-4, the surface remained in relatively good condition with no noticeable corrosion. These results verified that the stability of the passive film when welded with ERNiCrMo-4 had a similar level of corrosion resistance to that of the base metal, and the decreased corrosion resistance characteristics were displayed under the desulfurization equipment environment when welded with ERNiCrMo-3 filler metal.

TABLE 3 Results of cyclic potentiodynamic polarization tests of the specimens tested in green death solution at 60°C.

	E_{corr} (V/SCE)	i_{corr} (μA/cm^2)	E_{pit} (V/SCE)	E_{rep} (mVSCE)
Base metal	0.44	0.32	0.87	0.85
ERNiCrMo-4	0.41	0.91	0.86	0.87
ERNiCrMo-3	0.40	2.76	0.85	-

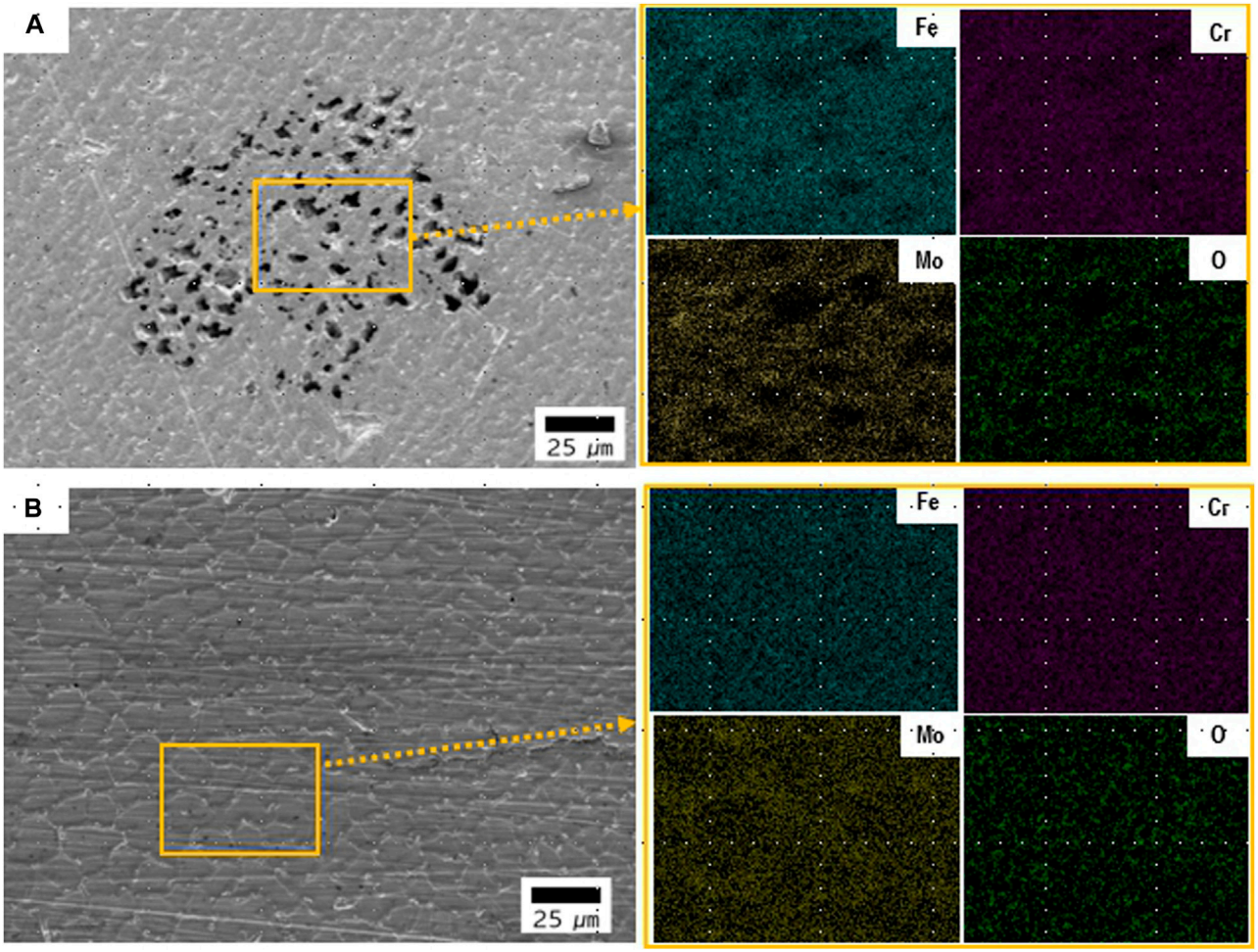

FIGURE 8
SEM morphologies with EDS mapping results after potentiodynamic polarization in the desulfurization equipment simulation environment **(A)** ERNiCrMo-3 filler metal **(B)** ERNiCrMo-4 filler metal.

3.3 Open circuit potential measurements

Figure 9 shows the changed current density when applying 0.5 V/SCE to the welded and fabricated test material for 1 h, which is the potential in the passive region, in the simulated desulfurization equipment environment by changing the type of filler metal. This figure verifies that current density tend to rapidly decrease when passive film is formed on the surface of all specimens (Lee and Bäßler, 2018; Lee et al., 2018). Figure 10 shows the potential behavior measured over time while maintaining the specimen in the open-circuit potential state under the desulfurization equipment environment after forming a passive by applying a constant potential. Here, the time that the potential is transitioned into the activation potential, that is, the time that is rapidly decreasing potential over time, is called the self-activation time, which refers to the state where the passive film is dissolved (Shibata, 2009). When welded with the ERNiCrMo-3 filler metal, the value gradually decreased over time from around 0.45 V/SCE, which is the sign of potential where the early passive film was formed, and the trend of rapidly decreasing value after approximately 10,000 s was

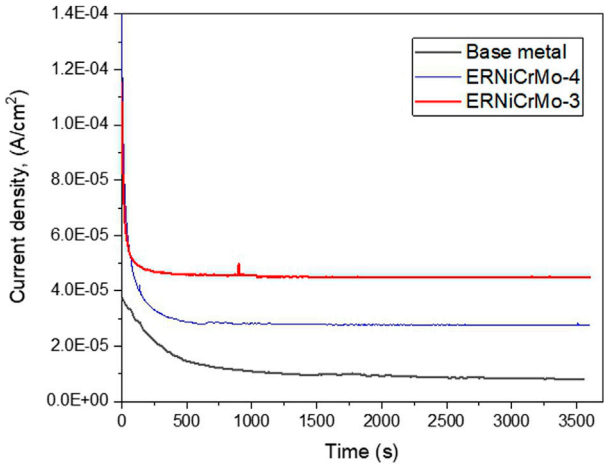

FIGURE 9
Current density for potentiostatic passivation process + 500 mV/SCE in the desulfurization equipment simulation environment.

verified. This meant the status of transition from the passive state into the re-activation state, which could be explained as a result of the reduction-dissolution of the passive film (Shibata, 2009). On the other hand, the base metal and the weldments using a ERNiCrMo-4 filler metal, the potential shows similar behavior to that of the beginning even after time has elapsed. This result verified that the stability of the passive film formed in the desulfurization equipment environment was more excellent when welded with ERNiCrMo-4 (Shibata, 2009).

3.4 Passive film analysis

The XPS analysis was conducted after the specimen was immersed in the desulfurization equipment environment to verify the characteristics of the passive film formed in the desulfurization equipment environment. Figures 11, 12 show the XPS composition analysis results of Fe2p, Cr2p, and Mo3d, which were found on the surface of the specimens before and after the weldment is exposed to the desulfurization equipment environment when using ERNiCrMo-3 and ERNiCrMo-4 filler metals. The corresponding binding energies (BEs) of the peaks and full-width at half-maximum (FWHM) values are given in Table 4.

As shown in Figure 11, the peak analysis results of the specimen welded with ERNiCrMo-3 filler metal verified that Fe before immersion existed in Fe_2O_3 (iron oxide) in the form of Fe(III) oxide and FeOOH (iron oxyhydroxide) in the form of hydroxide, but Fe in the passive film formed after exposure to the desulfurization equipment environment existed in Fe_2O_3 and Fe in the form of the metal state. For Cr, the same structure where Cr_2O_3 (Chromium oxide) in the form of Cr (III) oxide and metallic Cr coexist was verified before and after the immersion in the desulfurization equipment environment. For Mo, the existence of MoO_2 (Molybdenum dioxide) in the form of Mo(V) oxide, MoO_3 (Molybdenum trioxide) in the form of Mo(VI) oxide, and Mo in the form of the metal state was verified before and after the immersion.

As shown in Figure 12, the analysis results of the peak of the specimen welded with ERNiCrMo-4 filler metal exhibited that Fe was composed of Fe_2O_3 and FeOOH composition before the immersion, and most of Fe existed in Fe_2O_3 and Fe in the form of the metal state after the immersion in the desulfurization equipment environment. For Cr, the passive film was composed of Cr_2O_3 (Chromium oxide) in the form of Cr(III) oxide before and after the immersion, and Cr in the metal state, which was verified before the immersion, was not verified after exposure to the desulfurization equipment. For Mo, the passive film was composed of MoO_2, which accounted for the largest proportion along with MoO_3 and Mo in the form of the metal state before the immersion. However, Mo existed in the passive film mostly in the form of MoO_3 after the immersion.

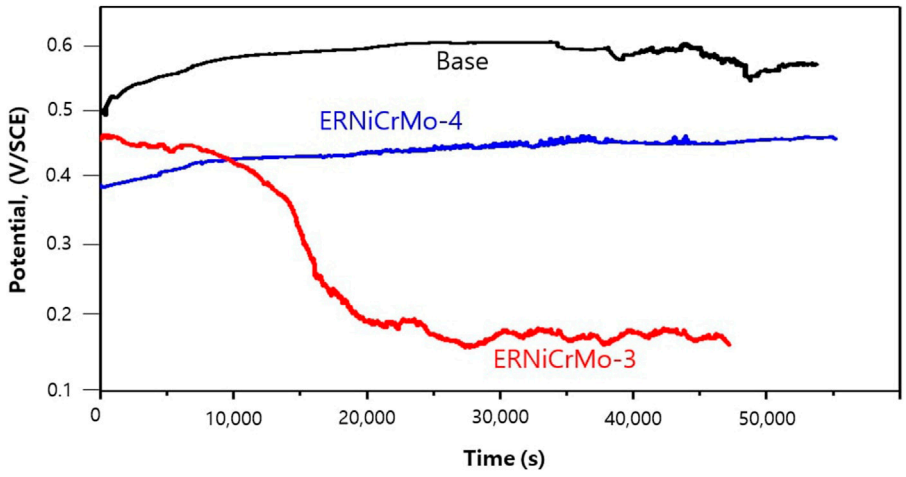

FIGURE 10
Open circuit potential curve in the desulfurization equipment simulation environment during self-activation process.

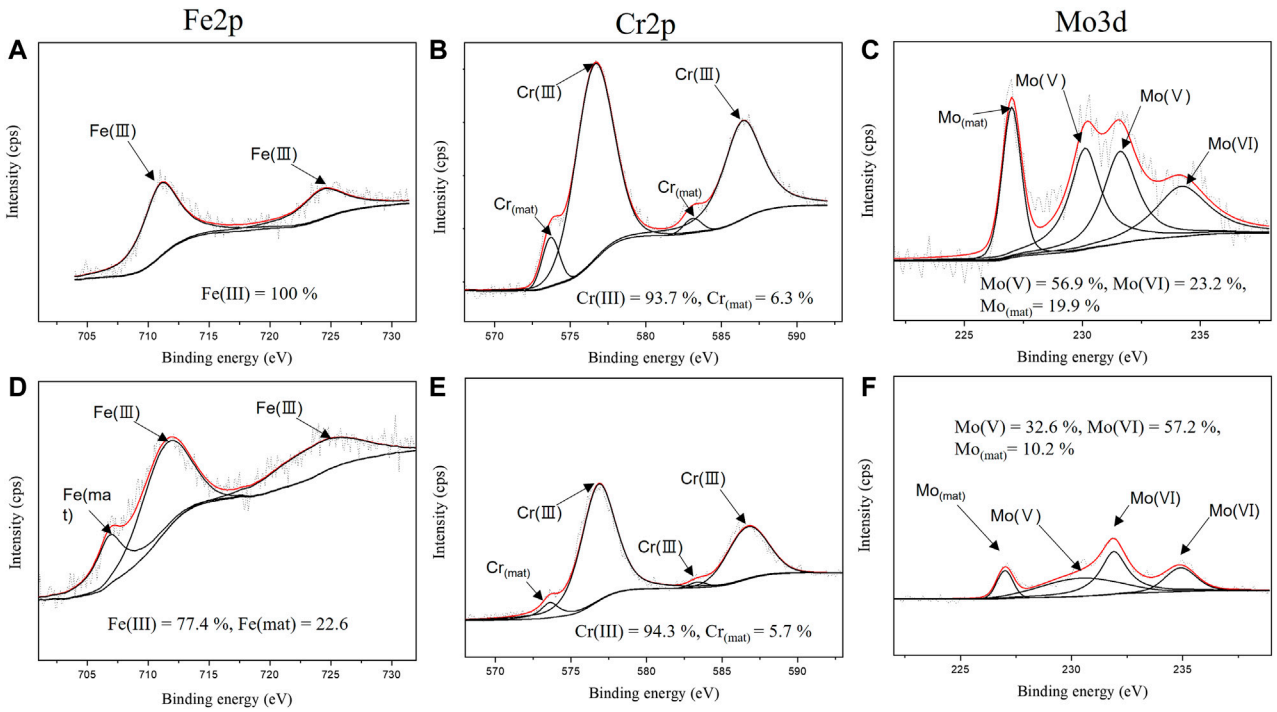

FIGURE 11
XPS spectra of Fe 2p, Cr 2p and Mo 3d of the surface for ERNiCrMo-3 filler metal: **(A–C)** original surface **(D–F)** after immersion 7 days in the desulfurization equipment simulation environment.

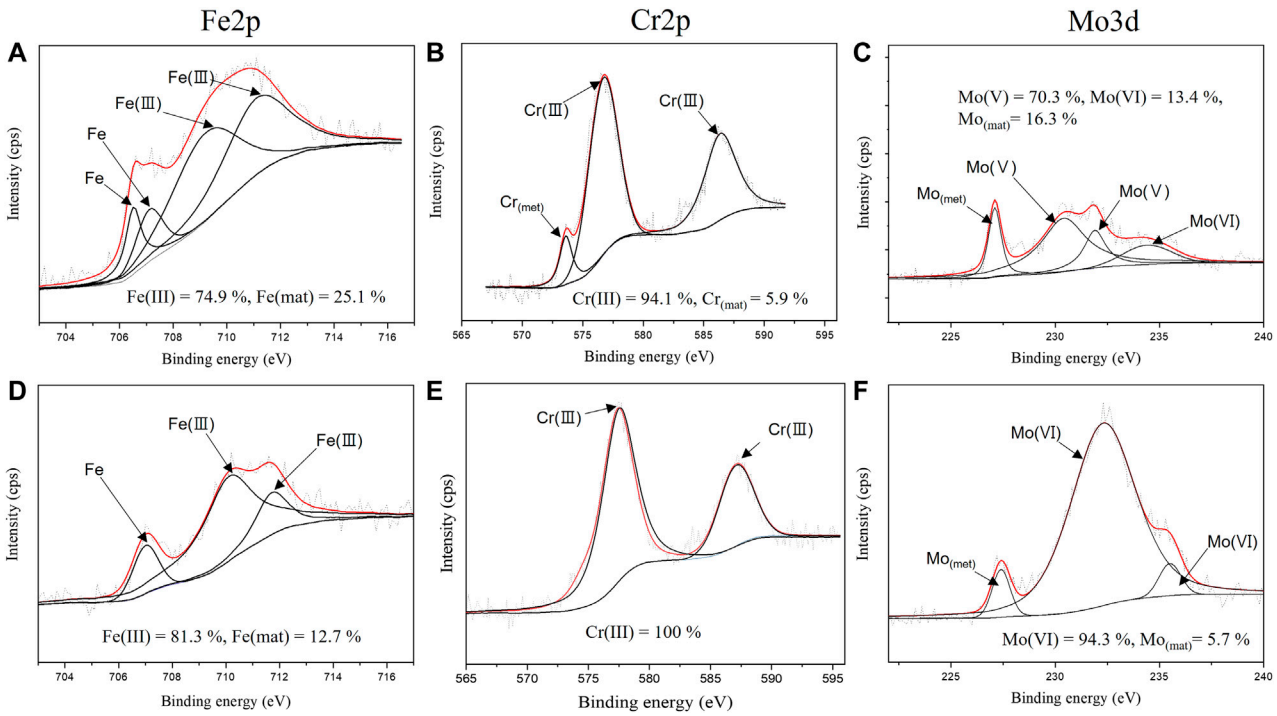

FIGURE 12
XPS spectra of Fe 2p, Cr 2p and Mo 3d of the surface for ERNiCrMo-4 filler metal: **(A–C)** original surface **(D–F)** after immersion 7 days in the desulfurization equipment simulation environment.

10.3389/fmats.2023.1038574

TABLE 4 Binding energies (BEs) and full-width at half-maximum (FWHM) values of the fitted components of the XPS peaks before and after in green death solution.

Immersion before							
ERNiCrMo-3				ERNiCrMo-4			
Element	Chemical state	BEs (eV)	FWHM (eV)	Element	Chemical state	BEs (eV)	FWHM (eV)
Fe 2p	Fe(III)	711.0	3.56	Fe 2p	Fe(III)	709.2	2.91
		724.3	4.55			711.1	2.93
	$Fe_{(mat)}$				$Fe_{(mat)}$	707.1	1.2
						706.5	0.71
Cr 2p	Cr(III)	576.6	2.95	Cr 2p	Cr(III)	576.7	2.84
		586.4	3.05			586.3	3.12
	$Cr_{(mat)}$	573.6	1.46		$Cr_{(mat)}$	573.6	1.26
Mo 3d	Mo(V)	230.1	1.56	Mo 3d	Mo(V)	230.4	2.61
		231.6	1.72			231.9	1.23
	Mo(VI)	234.2	2.67		Mo(VI)	234.4	2.71
	$Mo_{(mat)}$	226.9	0.96		$Mo_{(mat)}$	227.1	0.72
Immersion after							
Fe 2p	Fe(III)	711.1	4.66	Fe 2p	Fe(III)	710.1	2.36
		723.9	8.48			711.7	1.43
	$Fe_{(mat)}$	706.8	2.8		$Fe_{(mat)}$	707.0	1.12
Cr 2p	Cr(III)	576.8	2.68	Cr 2p	Cr(III)	577.4	3.16
		586.7	3.17			587.1	3.03
	$Cr_{(mat)}$	583.1	1.39		$Cr_{(mat)}$	574.5	2.65
Mo 3d	Mo(V)	230.4	4.18	Mo 3d	Mo(VI)	232.3	3.69
	Mo(VI)	231.9	1.45			235.5	1.23
		234.9	1.66		$Mo_{(mat)}$	227.4	1.01
	$Mo_{(mat)}$	227.0	0.86				

The corrosion resistance of super austenitic stainless steel in a strong acidic environment is greatly affected by Cr_2O_3 and MoO_3 (Sugimoto and Sawada, 1976; Yang et al., 1984; Hashimoto et al., 2007). The analysis results of the surface condition in the two specimens before and after immersion verified that the composition of Cr_2O_3 did not change significantly; The Cr_2O_3 ratios of ERNiCrMo-3 and ERNiCrMo-4 changed from 93.7% to 94.3% and 94.1% to 100.0% (Figures 11B, 12B). This indicates that the re-passivation of Cr oxide is proceeding stably due to the high Cr content on the entire weld surface in both specimens (Lee, 2006). On the other hand, in the case of Mo, the composition ratio was different depending on the structure according to the type of filler material; The MoO_3 ratio of ERRNiCrMo-3 and ERNiCrMo-4 increased from 23.2% to 57.2% and 13.4%–94.3%, respectively (Figures 11C, 12C). The difference of the form of MoO_3 which is a further oxidation of passive Mo film, is closely linked to Mo content (Lee, 2006). The high content of Mo facilitates stable passive film, causing faster repassivation (Lee, 2006). That is, through the result of the XPS analysis, in the case of ERNiCrMo-3 where Mo deficiency exists, repassivation is inferior to ERNiCrMo-4 with a high distribution of Mo on all surfaces.

3.5 Discussion

Table 5 presents the element composition in the microstructure of the specimen when using ERNiCrMo-3 and ERNiCrMo-4 filler metals along with the quantitatively calculated PREN. Table 5 verified that both materials welded with ERNiCrMo-3 and ERNiCrMo-4 filler metals had a difference in PREN in the dendrite and interdendritic regions. Particularly, this phenomenon was more evident in the weldment when using the ERNiCrMo-3 filler metal, and significant degradation with lower PREN than the base metal was also verified. In this study, a distinctive degradation of the corrosion resistance characteristics was also verified when the material in the region whose PREN significantly dropped was exposed to the desulfurization equipment environment. Through this identification, it was found that the

TABLE 5 Pitting resistance equivalent number (PREN) of the interdendritic region and the dendritic region and the difference of PREN between the two regions of difference filler metals.

Weld type	Region		Chemical composition (wt%)			PREN [a]	△PREN [b]
			Cr	Mo	N		
Base metal (UNS N08367)			20.6	6.4	0.3	50.8	-
GTAW ERNiCrMo-3	Weld metal	Interdendritic	18.9	14.7	—	67.5	+ 36.1
		dendritic	20.6	3.3	—	31.4	
	Weld interface	Interdendritic	20.7	9.6	—	52.4	+ 20.3
		dendritic	21.3	3.3	—	32.1	
GTAW ERNiCrMo-4	Weld metal	Interdendritic	22.1	12.5	—	63.2	+ 14.3
		dendritic	19.4	8.9	—	48.9	
	Weld interface	Interdendritic	20.8	9.9	—	53.5	+ 10.1
		dendritic	20.9	6.8	—	43.4	

[a]PREN = wt %Cr + 3.3 wt %Mo + 30 wt %N.
[b]△PREN = interdendritic region PREN—dendritic region PREN.

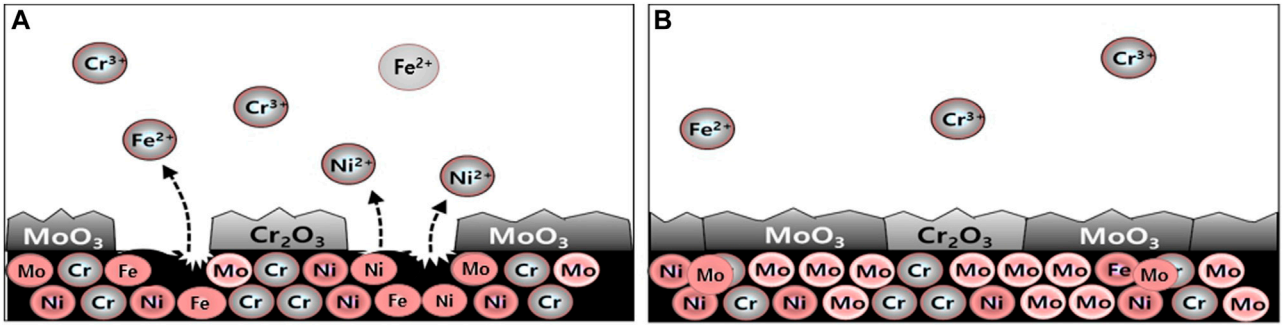

FIGURE 13
Corrosion mechanism proposed in the desulfurization equipment simulation environment: **(A)** ERNiCrMo-3 filler metal **(B)** ERNiCrMo-4 filler metal.

difference in the element composition distribution per microstructure had a closer relationship with the corrosion resistance characteristics of the material whichever exposed to the desulfurization equipment environment.

Furthermore, the difference in PREN resulting from this element deficiency is closely associated with the formation of a passivation film, which plays a crucial role in determining the corrosion resistance characteristics in the desulfurization equipment environment. Mo appears to be associated with the characteristic of the stable state composition of the MoO_2 form under neutral and slightly acidic environments as illustrated in the Pourbaix diagrams. Many previous studies reported that the oxide layer on the form of MoO_2 played a key role in protecting materials from aggressive ions (Sugimoto and Sawada, 1976; Kodama and Ambrose, 1977; Ogura and Ohama, 1984; Lu and Clayton, 1985; Brooks et al., 1986; Clayton and Lu,, 1986). However, for the weldment of super austenitic stainless steel exposed to a strong acidic environment, it was found that the MoO_3 oxide, which was stably formed on the surface, played the key role in maintaining the corrosion resistance characteristics of the material (Sugimoto and Sawada, 1976; Yang et al., 1984; Hashimoto et al., 2007).

Figure 13 presents a proposed mechanism that can explain the effect of the amount of Mo on the corrosion resistance of super-austenitic stainless steel in the desulfurization equipment simulation environment. In the case of ERNiCrMo-3 weldment, it was verified through XPS analysis that MoO_3, which played a pivotal role in the corrosion resistance, was formed unstably due to Mo segregation in the dendritic region. This effect led to a rapid decrease in the corrosion resistance of the welded part, as confirmed by cyclic polarization tests and observation of open circuit potential. Furthermore, the unprotected bulk material was exposed to an aggressive solution, resulting in localized corrosion attack, as shown in Figure 13A. On the other hand, in the case of ERNiCrMo-4 weldment, the Mo content was significantly maintained even after welding. As a result, XPS analysis confirmed the formation of a passive film containing MoO_3 on

the surface. Corrosion tests further demonstrated that this stable passivation film effectively protected the entire material from aggressive ions. Through this study, it was confirmed that the welding part in the desulfurization equipment achieved stable corrosion resistance through the formation of MoO_3, facilitated by a high content of Mo Figure 13B.

4 Conclusion

This study verified the correlation of the microstructure in the weldment of super austenitic stainless steel, which was joined by using two different types of filler metals, and changes in the condition of the element composition distribution with the corrosion resistance characteristics of the material. Also, it could verify the formation of the passive film when exposed to the desulfurization equipment-simulated environment. The following conclusions have been confirmed through our study carried out.

1. The Mo microsegregation toward the inter-dendritic within the fusion zone was observed at ERNiCrMo-3 and ERNiCrMo-4. However, the Mo microsegregation ratio was confirmed to be much larger for ERNiCrMo-3 than ERNiCrMo-4.
2. Corrosion studies in the desulfurization equipment environment showed that ERNiCrMo-4 had better corrosion resistance than ERNiCrMo-3, and even its properties were not significantly different from those of the substrate material.
3. The localized corrosion was found to start at the dendritic area that has low PREN because of the Mo microsegregation, and the range was propagated and spread. This was more clearly evident in ERNiCrMo-3 where a significant difference in PREN depending on microstructure was discernible.
4. This result was closely correlated with the formation of passive film in the form of MoO3 that can prevent aggressive ion intrusion as it was present in a stable state in a strong acidic environment such as when using desulfurization equipment, which was verified through XPS analysis.

In future studies, further studies about the evaluation of anti-corrosion characteristics of weldment when variously changing the conditions such as welding heat input, shielding gas, and post-treatment that may affect the anti-corrosion characteristics and mechanical properties are recommended.

Data availability statement

The raw data supporting the conclusion of this article will be made available by the authors, without undue reservation.

Author contributions

BS: Conceptualization, Methodology, Investigation, Writing—original draft. YK: Methodology, Investigation. SO: Methodology. SL: funding acquisition. ML: Supervision. All authors contributed to the article and approved the submitted version.

Funding

This research was a part of the project titled “The development of marine-waste disposal system optimized in an island-fishing village”, funded by the Ministry of Oceans and Fisheries, Korea.

Conflict of interest

The authors declare that the research was conducted in the absence of any commercial or financial relationships that could be construed as a potential conflict of interest.

Publisher’s note

References

Aragon, E., Woillez, J., Perice, C., Tabaries, F., and Sitz, M. (2009). Corrosion resistant material selection for the manufacturing of marine diesel exhausts scrubbers. *Mat. Des.* 30 (5), 1548–1555. doi:10.1016/j.matdes.2008.07.053

Astm, G. G. (2001). 61-86: Standard test method for conducting cyclic potentiodynamic polarization measurements for localized corrosion susceptibility of iron. *Nickel-, or Cobalt-Base Alloy. Annu. B. ASTM Stand.* 3, 223–227. doi:10.1520/G0061-86R18

Aulinger, A., Matthias, V., Zeretzke, M., Bieser, J., Quante, M., and Backes, A. (2016). The impact of shipping emissions on air pollution in the greater north sea region–Part 1: Current emissions and concentrations. *Atmos. Chem. Phys.* 16 (2), 739–758. doi:10.5194/acp-16-739-2016

Brooks, A. R., Clayton, C. R., Doss, K., and Lu, Y. C. (1986). On the role of Cr in the passivity of stainless steel. *J. Electrochem. Soc.* 133 (12), 2459–2464. doi:10.1149/1.2108450

Chacón-Fernández, S., Portolés García, A., and Romaní Labanda, G. (2022). Analysis of the influence of GMAW process parameters on the properties and microstructure of S32001 steel. *Mater. (Basel)* 15 (18), 6498. doi:10.3390/ma15186498

Clayton, C. R., and Lu, Yc. (1986). A bipolar model of the passivity of stainless steel: The role of Mo addition. *J. Electrochem. Soc.* 133 (12), 2465–2473. doi:10.1149/1.2108451

Crum, J. R., Shoemaker, L. E., and Stiltner, G. (1996). “The role of nickel alloys in fighting corrosion in wet limestone FGD systems,” in *Corrosion 96* (Denver, Colorado: OnePetro).

DeForce, B. (2017). “Evaluation of alloys for marine exhaust scrubbers,” in *Corrosion 2017* (Phoenix, Arizona, USA: OnePetro).

Dupont, J. N., Banovic, S. W., and Marder, A. R. (2003). Microstructural evolution and weldability of dissimilar welds between a super austenitic stainless steel and nickel-based alloys. *Weld. J.* 82 (6), 125.

Esmailzadeh, S., Aliofkhazraei, M., and Sarlak, H. (2018). Interpretation of cyclic potentiodynamic polarization test results for study of corrosion behavior of metals: A review. *Prot. Mater. Phys. Chem. surfaces* 54 (5), 976–989. doi:10.1134/s207020511805026x

Ezer, M. A., and Çam, G. (2022). A study on microstructure and mechanical performance of gas metal arc welded AISI 304 L joints. *Materwiss. Werksttech.* 53 (9), 1043–1052. doi:10.1002/mawe.202200050

Fang, Z., Zhang, L., Wu, Y. S., Li, J. Q., Sun, D. B., Jiang, G., et al. (1995). Thioacetamide as an activator for the potentiodynamic reactivation method in evaluating susceptibility of type 304L stainless steel to intergranular corrosion. *Corrosion* 51 (02), 124–130. doi:10.5006/1.3293584

Gong, Y., and Yang, Z.-G. (2018). Corrosion evaluation of one wet desulfurization equipment–flue gas desulfurization unit. *Fuel Process. Technol.* 181, 279–293. doi:10.1016/j.fuproc.2018.10.005

Guo, D., Kwok, C. T., Chan, S. L. I., and Tam, L. M. (2021). Friction surfacing of AISI 904L super austenitic stainless steel coatings: Microstructure and properties. *Surf. Coat. Technol.* 408, 126811. doi:10.1016/j.surfcoat.2020.126811

Ha, H., and Kwon, H. (2007). Effects of Cr2N on the pitting corrosion of high nitrogen stainless steels. *Electrochim. Acta* 52 (5), 2175–2180. doi:10.1016/j.electacta.2006.08.034

Hashimoto, K., Asami, K., Kawashima, A., Habazaki, H., and Akiyama, E. (2007). The role of corrosion-resistant alloying elements in passivity. *Corros. Sci.* 49 (1), 42–52. doi:10.1016/j.corsci.2006.05.003

Heino, S. (2000). Role of Mo and W during sensitization of superaustenitic stainless steel—crystallography and composition of precipitates. *Metall. Mat. Trans. A* 31 (8), 1893–1905. doi:10.1007/s11661-000-0217-9

Hertzman, S., Pettersson, R. J., Blom, R., Kivineva, E., and Eriksson, J. (1996). High nitrogen steels. Influence of shielding gas composition and welding parameters on the N-content and corrosion properties of welds in N-alloyed stainless steel grades. *ISIJ Int.* 36 (7), 968–976. doi:10.2355/isijinternational.36.968

Kang, J., Kim, T., Tak, Y., Lee, J., and Yoon, J. (2012). Cyclic voltammetry for monitoring bacterial attachment and biofilm formation. *J. Ind. Eng. Chem.* 18 (2), 800–807. doi:10.1016/j.jiec.2011.10.002

Kallinikos, L. E., Farsari, E. I., Spartinos, D. N., and Papayannakos, N. G. (2010). Simulation of the operation of an industrial wet flue gas desulfurization system. *Fuel Process. Technol.* 91 (12), 1794–1802. doi:10.1016/j.fuproc.2010.07.020

Kim, S.-T., Kim, S.-Y., Lee, I.-S., Park, Y.-S., Shin, M.-C., and Kim, Y.-S. (2011). Effects of shielding gases on the microstructure and localized corrosion of tube-to-tube sheet welds of super austenitic stainless steel for seawater cooled condenser. *Corros. Sci.* 53 (8), 2611–2618. doi:10.1016/j.corsci.2011.04.021

Kodama, T., and Ambrose, J. R. (1977). Effect of molybdate ion on the repassivation kinetics of iron in solutions containing chloride ions. *Corrosion* 33 (5), 155–161. doi:10.5006/0010-9312-33.5.155

Lauro, A., and Mandina, M. (2003). Welding and weldability of the 'super-austenitic'and 'super-Martensitic'Stainless steels. *Weld. Int.* 17 (9), 710–720. doi:10.1533/wint.2003.3149

Lee, J.-B. (2006). Effects of alloying elements, Cr, Mo and N on repassivation characteristics of stainless steels using the abrading electrode technique. *Mat. Chem. Phys.* 99 (2–3), 224–234. doi:10.1016/j.matchemphys.2005.10.016

Lee, J.-S., and Bäßler, R. (2018). Aging of passive film on UNS N08031 in a green-death solution. *Corros. Eng. Sci. Technol.* 53 (4), 302–308. doi:10.1080/1478422x.2018.1459077

Lee, J., Radnik, J., and Bäßler, R. (2018). Passivity of alloy 31 in green-death solution. *Mat. Corros.* 69 (9), 1218–1226. doi:10.1002/maco.201709996

Lu, Y. C., and Clayton, C. R. (1985). Evidence for a bipolar mechanism of passivity in Mo bearing stainless steels. *J. Electrochem. Soc.* 132 (10), 2517–2518. doi:10.1149/1.2113614

Makkonen, T., and Repka, S. (2016). The innovation inducement impact of environmental regulations on maritime transport: A literature review. *Int. J. Innov. Sustain. Dev.* 10 (1), 69–86. doi:10.1504/ijisd.2016.073413

Manikandan, S. G. K., Sivakumar, D., Rao, K. P., and Kamaraj, M. (2014). Effect of weld cooling rate on laves phase formation in Inconel 718 fusion zone. *J. Mat. Process. Technol.* 214 (2), 358–364. doi:10.1016/j.jmatprotec.2013.09.006

Miranda-Pérez, A. F., Rodríguez-Vargas, B. R., Calliari, I., and Pezzato, L. (2023). Corrosion resistance of GMAW duplex stainless steels welds. *Mater. (Basel)* 16 (5), 1847. doi:10.3390/ma16051847

Nagarajan, S., and Rajendran, N. (2009). Crevice corrosion behaviour of superaustenitic stainless steels: Dynamic electrochemical impedance spectroscopy and atomic force microscopy studies. *Corros. Sci.* 51 (2), 217–224. doi:10.1016/j.corsci.2008.11.008

Ogura, K., and Ohama, T. (1984). Pit Formation in the cathodic polarization of passive iron IV. Repair mechanism by molybdate, chromate and tungstate. *Corrosion* 40 (2), 47–51. doi:10.5006/1.3593909

Pan, P., Chen, H., Liang, Z., and Zhao, Q. (2017). Experimental study on corrosion of steels for flue gas reheaters in a coal-fired power plant. *Appl. Therm. Eng.* 115, 267–279. doi:10.1016/j.applthermaleng.2016.12.066

Paul, L., Wahl, V., and Alves, H. (2015). "Alloy options for shipboard scrubbers of diesel fuel emissions," in *Corrosion 2015* (Dallas, Texas: OnePetro).

Phull, B. S., Mathay, W. L., and Ross, R. W. (2000). "Corrosion resistance of duplex and 4-6% Mo-containing stainless steels in FGD scrubber absorber slurry environments," in *Corrosion 2000* (Orlando, Florida: OnePetro).

Rabensteiner, G. (1989). Welding of fully austenitic stainless steels with high molybdenum contents. *Weld. World* 27 (1), 2–13.

Rommerskirchen, I., Gutsch, M., and Mast, R. (2001). Einfluss der halbzeugform auf die korrosionsbeständigkeit hochlegierter Ni-Cr-Mo-werkstoffe. *Mat. Corros.* 52 (8), 625–628. doi:10.1002/1521-4176(200108)52:8<625::aid-maco625>3.0.co;2-8

Sathiya, P., Sudhakaran, A., and Soundararajan, R. (2012). Mechanical and metallurgical investigation on gas metal arc welding of super austenitic stainless steel. *Int. J. Mech. Mat. Eng.* 7 (1), 107–112.

Seifert, M., Siebert, S., and Theisen, W. (2016). Development of a powder metallurgical corrosion-resistant bearing steel containing NbC and its transfer to industrial applications. *Mat. Sci. Technol.* 32 (4), 313–319. doi:10.1080/02670836.2015.1118789

Şenol, M., and Çam, G. (2023). Investigation into microstructures and properties of AISI 430 ferritic steel butt joints fabricated by GMAW. *Int. J. Press. Vessel. Pip.* 202, 104926. doi:10.1016/j.ijpvp.2023.104926

Serindağ, H. T., and Çam, G. (2022b). Characterizations of microstructure and properties of dissimilar AISI 316l/9Ni low-alloy cryogenic steel joints fabricated by gas tungsten arc welding. *J. Mat. Eng. Perform.*, 1–11. doi:10.1007/s11665-022-07601-x

Serindağ, H. T., and Çam, G. (2022a). Multi-pass butt welding of thick AISI 316L plates by gas tungsten arc welding: Microstructural and mechanical characterization. *Int. J. Press. Vessel. Pip.* 200, 104842. doi:10.1016/j.ijpvp.2022.104842

Serindağ, H. T., Tardu, C., Kirçiçek, İ. Ö., and Çam, G. (2022). A study on microstructural and mechanical properties of gas tungsten arc welded thick cryogenic 9% Ni alloy steel butt joint. *CIRP J. Manuf. Sci. Technol.* 37, 1–10. doi:10.1016/j.cirpj.2021.12.006

Serindağ, H. T., and Çam, G. (2021). Microstructure and mechanical properties of gas metal arc welded AISI 430/AISI 304 dissimilar stainless steels butt joints. *J. Phys. Conf. Ser. IOP Publ.* 1777, 012047. doi:10.1088/1742-6596/1777/1/012047

Shibata, T. (2009). Critical factors for controlling the stability of the passive film on stainless steels. *ECS Trans.* 16 (52), 331–343. doi:10.1149/1.3229982

Shin, Y.-T. (2015). UNS S32654 for demanding offshore applications. *J. Weld. Join.* 33 (5), 9–13. doi:10.5781/jwj.2015.33.5.9

Standard, A. (2002). *A262-02a. Stand. Pract. Detect. Susceptibility to intergranular attack austenitic stainl. Steels*. West Conshohocken, USA: ASTM International, 1–17.

Stein, G., Hucklenbroich, I., and Feichtinger, H. (1999). Current and future applications of high nitrogen steels. *Mater. Sci. forum* 318, 151–160. doi:10.4028/www.scientific.net/msf.318-320.151

Sugimoto, K., and Sawada, Y. (1976). The role of alloyed molybdenum in austenitic stainless steels in the inhibition of pitting in neutral halide solutions. *Corrosion* 32 (9), 347–352. doi:10.5006/0010-9312-32.9.347

Taheri, A., Beidokhti, B., Shayegh Boroujeny, B., and Valizadeh, A. (2020). Characterizations of dissimilar S32205/316l welds using austenitic, super-austenitic and super-duplex filler metals. *Int. J. Min. Metall. Mat.* 27 (1), 119–127. doi:10.1007/s12613-019-1925-3

Woo, I., and Kikuchi, Y. (2002). Weldability of high nitrogen stainless steel. *ISIJ Int.* 42 (12), 1334–1343. doi:10.2355/isijinternational.42.1334

Wu, Y., Barton, S. C., and Lee, A. (2019). Galvanic corrosion behavior at the Cu-Al ball bond interface: Influence of Pd addition and chloride concentration. *Microelectron. Reliab.* 92, 79–86. doi:10.1016/j.microrel.2018.11.016

Yang, W., Ni, R.-C., Hua, H.-Z., and Pourbaix, A. (1984). The behavior of chromium and molybdenum in the propagation process of localized corrosion of steels. *Corros. Sci.* 24 (8), 691–707. doi:10.1016/0010-938x(84)90059-3

Ye, W., Li, Y., Long, K., Ren, M., and Qiang, H. A. N. (2013). Feasibility of flue-gas desulfurization by manganese oxides. *Trans. Nonferrous Mater. Soc. China* 23 (10), 3089–3094. doi:10.1016/s1003-6326(13)62838-1

Zhang, Y., and Li, J. (2012). Characterization of the microstructure evolution and microsegregation in a Ni-based superalloy under super-high thermal gradient directional solidification. *Mat. Trans.* 53 (11), 1910–1914. doi:10.2320/matertrans.m2012173

Zhu, J., Ye, S., Bai, J., Wu, Z., Liu, Z., and Yang, Y. (2015). A concise algorithm for calculating absorption height in spray tower for wet limestone–gypsum flue gas desulfurization. *Fuel Process. Technol.* 129, 15–23. doi:10.1016/j.fuproc.2014.07.002